Breach detection in spine surgery based on cutting torque

Elie Saghbiny, Lilyan Leblanc, Antoine Harlé, Christina Bobbio, Raphael Vialle, Guillaume Morel, Brahim Tamadazte

Breach detection in spine surgery based on cutting torque

E. Saghbiny*[1,2], L. Leblanc*[1], A. Harlé[1], C. Bobbio[1], R. Vialle[1,2], G. Morel[1], and B. Tamadazte[1]

***Abstract*—The accurate placement of pedicle screws is crucial for various spinal interventions, demanding precise geometric alignment while carrying inherent risks. Studies show that the rate of complications can reach up to 18% in case of imprecise placement of pedicle screws. To enhance the precision and safety of pedicle screw placement, we have developed a robotic system equipped with several sensors and paired with a breach detection algorithm capable of identifying potential breaches in the spinal canal. The breach detection algorithm was conceptualized through an analysis of the cutting torque of the drill system.**

An ex-vivo experiment was conducted to assess the effectiveness of the developed robotic solution and breach detection algorithm. The data (e.g., cutting torque, position, velocity, etc.) used during the validation were collected by drilling 80 pedicles in fresh porcine vertebrae.

The results demonstrated that the proposed algorithm could predict breaches in 96.42% of cases, i.e., the distance between the detected point (drilling stop) and the point of the breach is within 2 mm. In a single instance, the detection occurred earlier than anticipated due to the trajectory being oriented significantly medially, resulting in an initial interaction with the cortical bone at an earlier point.

***Index Terms*—Spine Surgery, Breach Detection, Medical Robotics, Robot Control, Torque.**

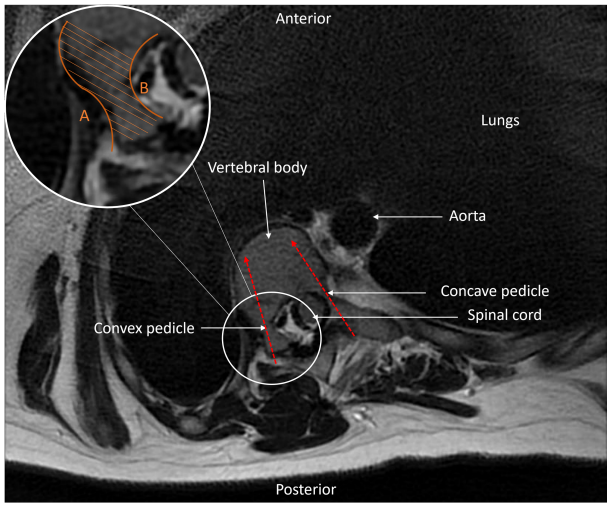

Fig. 1. An axial MRI section image illustrating alterations in traditional anatomical reference points. The zoomed area shows the structure of the pedicle, with cortical bone (A and B) and cancellous bone (shaded area). Dashed arrows illustrate the ideal trajectory for a screw through the pedicle.

I. INTRODUCTION

SCOLIOSIS represents a three-dimensional deformity characterized by distortions in the coronal, sagittal, and axial planes [1]. In addition to the geometric deformities, there is an anatomical alteration in the pedicles. On the concave side, the pedicles are notably slender, and the spinal cord is close to the medial wall of the pedicle (Fig. 1).

Pedicle screws are employed in the correction of deformities and wield significant corrective capacity by engaging all three structural columns of the vertebra. These screws are initially introduced through the posterior column, traverse the middle column formed by the pedicle, and ultimately anchor into the anterior column represented by the vertebral body. Pedicle preparation is a challenging procedure. The surgeon inserts screws from the posterior column while seeing solely the posterior aspect of the spine (Fig. 2). In scoliosis surgery, this task is particularly challenging due to the presence of vertebral rotation, pedicle deformation, and the intricate proximity to critical anatomical structures like the aorta and the spinal cord or spinal roots. A breach into the spinal canal can lead to spinal cord injury. Clinical symptoms range from mild muscle weakness and sensory loss to complete paraplegia. The consequences of a breach of the pedicular screw within the spinal canal depend on the extent of the screw's penetration into the canal. One of the most commonly used classifications to quantify this breach and predict its impact on the spinal cord and spinal roots is that proposed by *Gertzbein and Robbins* [2]. This classification involves assessing the degree of screw penetration into the spinal canal. The transpedicular screw position is graded from *A* to *E* based on the extent of the breach of the pedicle cortex:

- "*A*": Fully intrapedicular position without breaching the pedicle cortex;
- "*B*": Exceeding the pedicle cortex by less than 2 mm;
- "*C*": Exceeding the pedicle cortex by 2-4 mm;
- "*D*": Exceeding the pedicle cortex by 4-6 mm;
- "*E*": Exceeding the pedicle cortex by more than 6 mm or being located outside the pedicle.

Grades "*A*" and "*B*" are typically regarded as satisfactory outcomes in surgical procedures. However, in cases graded from "*C*" to "*E*", there is a potential for neurological symptoms to manifest, which can contribute to unsatisfactory surgical results. Notably, neurological damage can be delayed in instances of medial breaches [3].

In addition to neurological damage, reports of pulmonary

This work has been supported by EU's H2020 research and innovation program under grant agreement No. 101016985 (FAROS project)

* the authors contributed equally to this work.

[1] are with ISIR, UMR 7222 Sorbonne University, CNRS, U1150 INSERM, Paris, France.

[2] are with Sorbonne Université, Groupe de Recherche Clinique "Robotique et Innovations Chirurgicales" (GRC33), Hôpital Armand-Trousseau 26 Ave du Docteur Arnold Netter, 75012 Paris, France. elie.saghbini89@gmail.com

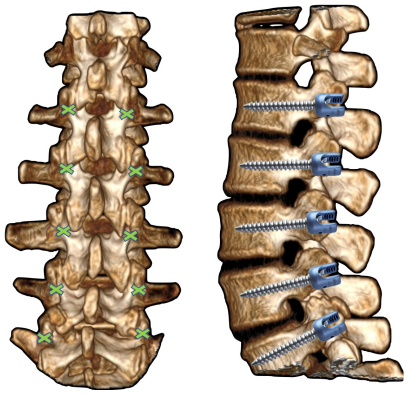

Fig. 2. Illustration of the entry point and the direction of the pedicle aim.

complications have also been noted [4]. Vascular injuries, including conditions such as false aneurysms [5], iatrogenic thoracic aortic injuries that require endovascular intervention [6], and delayed manifestations of aortic injury or perforation [7], have been documented.

This paper is structured as follows: Section II provides an overview of pedicle screw placement techniques, accuracy rates, and contributions. Section III discusses the experimental robotics platform and data collection methodology. Section IV presents the proposed breach detection algorithm using the drilling torque signal. Section V assesses our method using data from drilling 80 fresh pig vertebrae, examine its limitations and explores potential applications in other surgical areas. Finally, Section VI presents the conclusion and future outlook.

II. RELATED WORK

Perforation rates for pedicle screws in scoliosis surgery range from 1.2% to 65% [8]. This wide range is attributed to the different techniques used for detecting perforations. In studies utilizing plain radiographs, the range of misplacement is relatively low (1.2% - 3.0%) [9], [10]. Conversely, in studies where a CT scan was used to assess screw position, the rate is higher and may reach 65%. In a recent study, Kwan et *al.* [8] conducted a retrospective review of 140 scoliosis patients with a total of 2020 screws. The assessment of screw position was evaluated with a CT scan. The overall total perforation rate was 20.3% (410 screws) with 8.2% (166 screws) grade 1, 2.9% (58 screws) grade 2, and 9.2% (186 screws) grade 3 perforations. This study categorised perforations according to Rao et *al.* [11], following the same classification system as *Gertzbein and Robbins*. Given the multitude of potential complications, this highlights the critical importance of precise placement of pedicle screws.

Various techniques are employed to enhance the safety of pedicle screw placement, often involving surgical assistance. The freehand technique is the oldest and requires a perfect knowledge of the anatomy and a long learning curve. In assisted techniques, some methods are based on imaging technologies, while others are imageless, such as:

- 3D printed models, which assist the surgeon during surgical planning and procedures [12];
- 3D printed guides, which are used as patient-specific pedicle screw templates [13];
- Electrical conductivity signal, whose variations are determined by the conductivity of tissues being drilled and can alert the surgeon of imminent breach [14], offering 100% of breach detection [15];
- Somatosensory evoked potentials (SEPs), a neurophysiological monitoring method that measures the electrical responses of the brain and spinal cord to sensory stimuli, providing real-time feedback on the integrity of sensory pathways during surgery;
- Different types of exteroceptive sensors have also been investigated, such as vibroacoustic, accelerometer, bearing force, etc.
- Full-power drill, a technique that relies on the surgeon's experience and tactile feedback to determine the appropriate drilling depth and force, minimizing the risk of breaching the spinal canal.

The image-guided techniques are fluoroscopy-based navigation, CT-based navigation, robot-assisted, or ultrasound-guided.

De Vega et *al.* [16] recently published a systematic review and meta-analysis on the accuracy of different methods of pedicle screw placement. All the trials utilized the freehand method as a control group, except for one that used fluoroscopy-based navigation as a reference [17]. The accuracy of the modified free-hand method using electrical conductivity is superior to the standard free-hand method (95.96% versus 85.8%) [18]. The modified free-hand methods significantly increase accuracy compared to the traditional free-hand approach. Even when compared to fluoroscopy-based navigation, the modified freehand using a 3D model demonstrates higher accuracy (93.5% versus 84.7%, p-value = 0.0003) [17]. The 3D-printed anatomical model provides the surgeon with a better understanding of the anatomy of the deformed vertebrae [19]. Fluoroscopy-based and CT-based navigations are the two most common methods practised today. The literature supports that CT-based navigation improves the accuracy of pedicle screw placement. Compared to the free-hand method, CT-based navigation shows higher accuracy (94.08% accuracy rate in CT-based navigation compared to 86.39% accuracy rate in free-hand, odds ratio OR = 2.50, p-value = 0.02) [20]. CT-based navigation has the highest accuracy rate (95.5%) compared to other methods such as robot-assisted, fluoroscopy, and free-hand (90.5%, 91.5%, and 93.1% respectively) [21]. Although navigation and robotics have contributed significantly to advancements in spinal surgery, they have several limitations, particularly in terms of user-friendliness and precision. Patient respiratory movements can notably compromise precision, as even minor variations in the patient's position during pedicle preparation can lead to registration errors [22]. Moreover, these techniques rely on ionizing radiation, posing risks to the patient, surgeon, and medical staff [23]. Younger patients are more susceptible to the effects of radiation due to higher division rates, and those who received radiation in childhood have an increased risk of malignancy [24].

The use of a power drill in spine surgery is limited. Recent

literature showed that power drill does not affect the accuracy or the surgery time [25], [26]. The control of drilling relies on the experience of the surgeon; in experimental studies, surgeons drill beyond the far cortex by an average of 6.33 mm [27]. Today, no specialised technology is integrated into drilling tools designed to detect or minimize pedicle breaches. Bone breach detection was studied in cows' femur [28]. The detection method is based on Proportional and Derivative (PD) motion control coupled with the force control system in real-time drilling. High-pass filtering was applied to the thrust force, allowing it to detect the interface between bone layers and detect breaches [29]. Brett et *al.* developed one of the first algorithms for ear surgery [30]. Their approach identified a transition between layers when specific threshold values in the increased cutting torque and decreased penetration force were attained. In the study conducted by Torun et *al.*, torque was employed to identify breaches in cortical bone. Their methodology relied on the closed-loop approach utilizing force sensor data. The accuracy achieved on synthetic bone was 96.9$\pm$ 0.8 $\%$ while on sheep femur, it reached 98.1 $\pm$ 0.2 $\%$ [31]. The friction between the drill bit and the bone generates vibrations that vary depending on the bone density. When the drill crosses an interface (cancellous bone / cortical bone), the change in vibration is abrupt. Wang et *al.* relied on this change to detect a cortical breakthrough. Their study was conducted on bovine [32]. Based on their research, the automated drill demonstrated time savings of 30 to 60 $\%$ compared to manual drilling and enhanced surgical precision. The study was conducted using bovine femoral diaphyses. Given the femoral cortical bone's substantial thickness, the bone density disparity is significant. Using acoustic signals to identify breakthroughs and classify states has shown promise as a method for monitoring surgical drilling procedures [33]–[37]. Zakaria et *al.* [33], [34] achieved approximately 80 $\%$ accuracy when drilling into bovine bone. Their method utilized air-borne microphones, a factor problematic in real operating rooms due to their proximity to sterile and noisy environments. Additionally, they focused on long bone diaphyses, such as the tibia, characterized by thicker and denser cortical bone compared to cancellous bone. In a recent investigation conducted by Seibold et *al.* [38], contact microphones were employed on human cadaveric specimens, resulting in a sensitivity of 93 $\%$ through the application of a deep learning approach. Their research focused on human femurs. Massalimova et *al.* [39] recently published a study on breach detection in the spine using several types of sensors: a contact microphone, a free-field microphone, a tri-axial accelerometer, and a uni-axial accelerometer attached to the spine. The study revealed that the best results obtained with a single sensor were achieved using the contact microphone attached to the skin, which detected breaches with an 85.8 $\%$ success rate, and the uni-axial accelerometer, which achieved an 81 $\%$ detection rate. Furthermore, by combining the data from these two sensors, the researchers were able to enhance the breach detection accuracy to 98 $\%$, demonstrating the effectiveness of multi-sensor integration in spinal breach detection. In their recent state-of-the-art paper, Timmermans et *al.* reviewed non-radiative, non-visual spine sensing methods for breach detection. They reported that the use of different sensing methods integrated into robotic systems is common, achieving a detection rate of around 90 $\%$. Additionally, they suggested that the integration of multiple tools could further increase detection rates [40].

Nonetheless, drilling into the pedicle comes with its own set of challenges. The cancellous and cortical layers have different biomechanical traits, and these can vary from one patient to another. Also, precision is crucial during pedicle drilling due to its closeness to important anatomical structures. This makes it especially tough to identify breakthroughs in the spinal canal, requiring special detection strategies. The quality of the bone through which the drill bit cuts during drilling progression is a crucial factor in detecting breaches, making torque a reliable indicator for this purpose. The torque of a drill represents the force it can exert on an object. It is essentially the rotational force applied to the drill bit, thereby facilitating the drilling process. This rotational force originates from the drill's motor and is subsequently transferred through the drill bit. Specifically, the torque of a drill represents the force applied by the drill bit to the material being worked on, and as torque increases, so does the force exerted on the material.

The main contributions of the paper concern the development of a robotic platform for pedicle screw placement in the spine. The platform is equipped with a multitude of sensors to record drilling progress in the pedicles. Among the signals used is torque, which provides information on the layers traversed during drilling. As a result, we have developed an algorithm for detecting breaches in the spinal canal, which can prevent them in 96.42% of cases. This algorithm could be integrated into a spinal surgical workflow for safer pedicle preparation.

III. MATERIALS AND DATA COLLECTION

In this Section, we will introduce our robotic platform. We employed force control to sustain contact between the drill and the vertebra, thus averting slippage through the bone. Data collection involved drilling on 80 pig vertebrae under conditions resembling those of an operating room. Lastly, we will detail the algorithm devised for the real-time detection of cortical breaches in the spinal canal.

A. Robotic Platform for Spinal Surgery

Our robotic platform for pedicle screw placement is equipped with a customized KUKA LBR Med 7 R800 redundant robotic arm designed to meet healthcare specifications. It incorporates integrated joint torque, position and velocity sensors, a custom-made power drill, and a threaded drill bit. With a maximum payload capacity of 7 kg, it exhibits precise positional accuracy within $\pm$0.15 mm and offers seven degrees of freedom, allowing for joint redundancy (Fig. 3). During ex-vivo drillings, the vertebra is rigidly fixed with a clamp in a transparent box. A camera is fixed in front of the spinal canal to record the whole drilling procedure (Fig. 5). The utilized drill bit is composed of a 3 mm diameter cutter with a pyramidal tip and a threaded shaft. The threaded design of the drill ensures continuous contact between the drill and

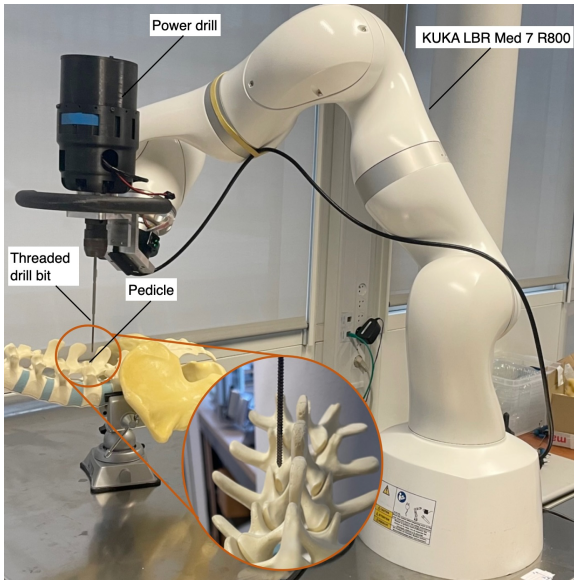

Fig. 3. Illustration of the developed robotic setup for pedicle screw placement.

the bone, preventing unintended motion along the z-axis, i.e., along the drilling path. A customized power drilling unit is employed for the drilling process, capable of delivering a nominal torque of 1.5 N·m and a maximum speed of 922 rotations per minute (rpm), enabling both drilling and screwing operations. Ultimately, the drilling system is affixed to the robot's end-effector at a 30° angle relative to the last robot axis, as depicted in Fig. 3.

B. Pseudo-force Controller

Pedicle drilling implies potential interactions between the robot, the clinical staff, and an unknown environment (i.e., vertebrae). Impedance control [41] is a widely used approach to enable safe interactions for human-robot cooperative tasks. Its goal is to realize the same dynamical relationship as a mass-spring-damper system with desired inertia, stiffness, and damping.

In impedance control, the dynamic relationship between the end-effector Cartesian pose vector $\boldsymbol{x} \in \mathbb{R}^6$ and the end-effector generalized interaction force $\boldsymbol{F_e} \in \mathbb{R}^6$ is:

$$\boldsymbol{\Lambda}_d\ddot{\mathbf{x}} = \mathbf{K}_d(\mathbf{x}_r - \mathbf{x}) + \mathbf{B}_d(\dot{\mathbf{x}}_r - \dot{\mathbf{x}}) - \boldsymbol{F}_e \ , \tag{1}$$

where $\boldsymbol{\Lambda}_d$, $\mathbf{B}_d$, $\mathbf{K}_d$, and $\mathbf{x}_r$ represent the desired inertial, damping, stiffness matrices, and the reference Cartesian position, respectively.

Regulating the interaction force to its desired value $\boldsymbol{F}_d$ requires adjusting $\dot{x}_r$ in real-time. A common approach seen in the literature is to implement an external force loop based on F/T sensor measurements as follows [42]:

$$\dot{\mathbf{x}}_r = \lambda(\boldsymbol{F}_d \ - \boldsymbol{F}_e) \ , \tag{2}$$

where λ is a proportional gain and $\boldsymbol{\tau_e}$ is the force measured at the end-effector level using an external force sensor.

To maintain stability, force control methods usually necessitate a reasonable estimation of the environment to accommodate contact dynamics. In spine surgery, the patient's

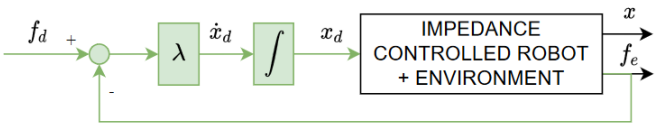

Fig. 4. Block diagram of the used pseudo-force control strategy.

position is unknown and variable (due to other signs such as breathing movements). Additionally, knowing beforehand the stiffness of contact seems not feasible. Consequently, conventional impedance control may engender instability in pedicle drilling. In this study, we implemented pseudo-force control to achieve consistent and stable force control during pedicle drilling as outlined in [43]. In this work, the authors show that better stability is achieved by defining a pseudo-force signal $\widetilde{\boldsymbol{F}}_{\boldsymbol{e}} = K_d(\mathbf{x}_r - \mathbf{x})$ as the feedback signal. This pseudo-signal feedback is illustrated in Fig. 4 and allows to define a new force regulation:

$$\dot{\mathbf{x}}_r = \Lambda\Big(\boldsymbol{F}_d - K_d(\mathbf{x}_r - \mathbf{x})\Big) \ . \tag{3}$$

where Λ is a diagonal matrix whose elements denote the proportional gains $\Lambda = diag(\lambda_1, ..., \lambda_6)$.

In our application, gains λ_i are set to zero for directions where the force is not controlled, leaving it free for conventional trajectory control, similar to hybrid position/force control. This pseudo-force control allows the application of a stable, constant force along a drilling direction on a vertebra of unknown position and stiffness while also rejecting undesirable high-frequency disturbances.

C. Data Collection and Labeling

The torque (respectively, position, velocity and time) data acquisition was performed on fresh pig lumbar vertebrae (a total of 80) obtained from a butcher shop. We opted for the pig model due to its close resemblance to humans despite variations in size and bone density. Knowing that the pedicle size and bone density differ between pigs and humans, the difference between the consistency of cancellous bone and cortical bone always exists. The trajectory direction was determined manually by the surgeon to ensure convergence and breach in the spinal canal to collect the torque from cortical breakthrough. The ex-vivo specimens, once at room temperature, were fixed in a clamping vice positioned within a clear box. A camera was strategically placed just outside the box to capture and monitor the internal aspects of the spinal canal, specifically to identify any occurrences of bone breaches. A surgical expert subsequently conducted a comprehensive review of the recorded videos and annotated the precise time of perforation. An example of annotation is represented in Fig. 5.

A few drilling parameters were defined in advance in discussion with clinicians. As a result, the drilling speed is fixed at 30 rpm, and the robot is force controlled with an initial desired force of f_d = 10 N and increased as needed to continue drilling. Numerous data signals were gathered,

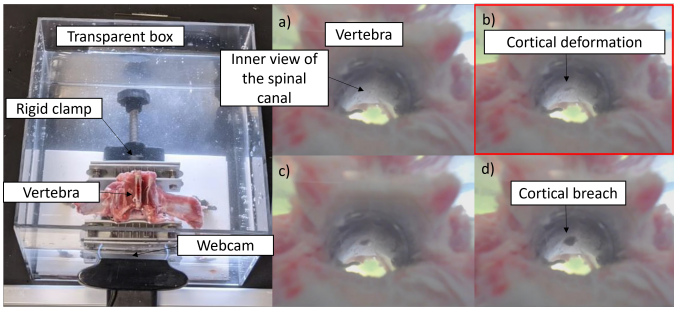

Fig. 5. On the left, we can see the setup; a webcam is filming the inside of the spinal canal. The right mosaic shows the deformations and bone penetration within the vertebral column while using the threaded instrument. There is no breach in the image (a); the image highlighted in red (b) denotes the moment the tool begins to exit the bone and enter the spinal canal. In images (c) and (d), we can see a progression of the tool through the cortical bone.

encompassing the robot's position for instrument depth calculation, drill torque, velocity, and time. This experiment's recording frequency for torque data is f = 45 Hz.

Note that for each signal, the surgeon defined the exact time instant of perforation by a posterior visualizing the videos recorded by the camera during the drilling (Fig. 5). This task allows grading perforation detection according to our derivation of the *Gertzbein-Robbins* classification. Detecting an imminent breaching before the actual point of perforation corresponds to grade "*A*" while declaring a perforation less than 2 mm after the actual perforation point corresponds to grade *"B"*. In other words, the detection is considered acceptable if a breach alert is raised before the right-most limit of the red area in Fig. 6.

IV. BREACH DETECTION METHOD

A. Torque Signal

Therefore, a clinically relevant bone breach detection algorithm should possess several characteristics. It must operate online, processing in real-time torque signals, which are inherently highly noisy. This noise prohibits the use of straightforward methods, such as gradients, to detect local or global maxima and necessitates filtering, which must introduce minimal delay. Additionally, the quality of cortical bone varies from one vertebra to another, meaning an absolute value cannot serve as a threshold. Consequently, a detection strategy that can adapt to varying torque profiles is essential.

The detection method was developed utilizing unfiltered torque values extracted directly from the drilling unit. Recognizing that cortical bone exhibits greater hardness compared to cancellous bone; it is theoretically anticipated that a noticeable increase in torque values will occur as the drill bit progresses. This signifies the need for heightened torque to sustain effective drilling until the far cortex's cortical bone is penetrated. Figure 6 illustrates various recorded torques during the drilling of fresh pig vertebrae. As expected, the torque signals are highly noisy, yet they all share a common feature: a gradual increase as the drill navigates through the cancellous bone, peaking to indicate contact with the cortical bone, followed by a gradual decrease post-breach. The vertical green lines show where the surgeon saw the breach on the recorded videos (Fig. 5(b)), and the red zone is the safe zone in which the position of the drill does not represent a risk to the patient according to the classification *Gertzbein and Robbin*.

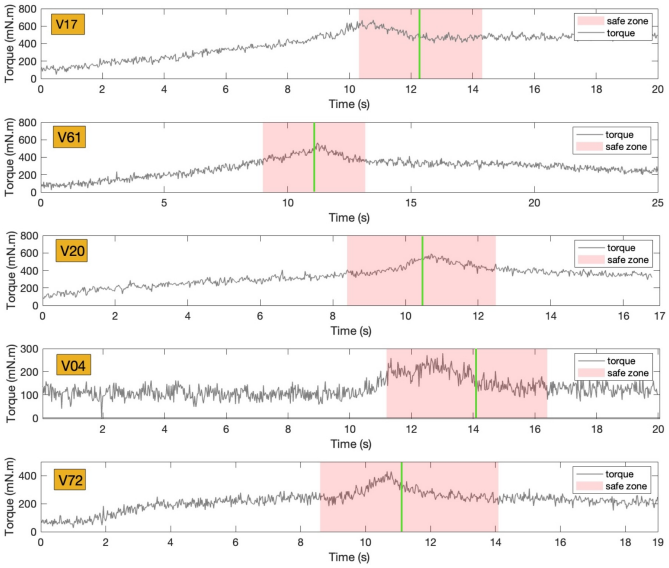

Fig. 6. Illustration of some recorded torques (for the vertebrae n° 17, 61, 20, 04 and 72). The red area represents the safe zone the surgeon defines around the moment the breach begins (vertical green line).

B. Data Online Processing

Among the common online noisy signals filtering approaches, the *Chebyshev* filter is renowned for its unusual characteristics. It recognizes a trade-off, in contrast to some other filters that place a higher priority on a smooth response. This type of filter attains interesting precision within its designated range by allowing controlled oscillations, also known as ripples, in the pass band. Consequently, the *Chebyshev* filter is utilized to process the raw torque signals, aiming to delineate significant patterns effectively [44].

Let us introduce the function of the *Chebyshev* filter as it is implemented in our case. The gain (or amplitude) response $G_n(\omega)$ of a *Chebyshev* n^{th}-order low-pass filter is given by:

$$G_n(\omega) = \frac{1}{\sqrt{1+\varepsilon^2 T_n^2(\omega/\omega_0)}} \ ,$$

where ω is the angular frequency, ε is the ripple factor in decibel (dB), ω_0 is the cutoff frequency, and T_n is a *Chebyshev* polynomial of the n^{th} order. The pass-band exhibits equiripple behaviour, with the ripple determined by the ripple factor ε.

The drill rotation speed is set at 30 rpm. Since controlling the rotation speed controls the insertion speed directly once the threads are engaged inside the bone, this equates to an insertion speed of 0.5 mm/second. Assuming that a significant drop in the torque signal is concurrent to a cortical bone breach, it is considered acceptable to introduce a delay of approximately 1 s when filtering the torque. Thus, ω_0 is set at 0.66 Hz. Manual tuning revealed that order $N = 4$ delivers good noise filtering and extracts the most meaningful signal variations. Finally, choosing a ripple factor $\varepsilon = 0.5$ dB limited

signal distortion and allowed us to apply our detection strategy efficiently.

C. Breach Detection Algorithm

Let us consider e to be the difference (in millimetres) between the depth z_v of the instrument at the breach time detected by the video and the depth z_a of the instrument at the instant t detected by our breach detection algorithm, i.e. $e = z_v - z_a$. $e > 0$ mm and $-2 < e < 0$ mm, therefore correspond to a grade "*A*", respectively to a grade "*B*", screw position according to the *Gerzbein-Robbins* classification. Thus, an algorithm is considered successful if all errors e are greater than -2 mm. In this study, the data were divided into a tuning set (30%) and a validation set (70%). Raw torque signals recorded during the ex-vivo pedicle drillings were streamed to emulate real-time pedicle drilling and test the breach detection algorithm. The spinal canal's bone consists of cortical bone, which is relatively harder and denser than the pedicle's trabecular bone. Consequently, there is a logical progression of torque increase when transitioning from cancellous bone to cortical bone, followed by a gradual decrease. The algorithm's objective is to identify Online this pattern of increasing and decreasing torque within an acceptable time-frame, aiming to prevent delayed detection. For each new value of the torque obtained at time t, we apply the *Chebyshev* filter with c_t the value of the resulting filtered torque. We then calculate the first derivative, $c'(t) = \frac{dc(t)}{dt}$. We define the following conditions which are required to trigger a breach detection:

- ***Condition 1***: The signal has consistently shown a decrease throughout a specified time interval $\Delta t_{decrease}$ preceding the present moment:
$$\forall t_n \in [t - \Delta t_{decrease}, t] : c'(t_n) < 0$$
- ***Condition 2***: The signal is currently exhibiting a decrease: $c'(t) < \delta_1$
- ***Condition 3***: If condition 1 and condition 2 are met, t_x is the latest time such that $c'(t_x) = 0$. Let $t_i = t_x - \Delta t_{increase}$, where :
$$d = c(t_x) - c(t_i) > \delta_2$$
- ***Decision***: If *Condition 1*, *Condition 2*, and *Condition 3* are true then **a breach is detected**.

The parameters used to tune the detection algorithm are : $\Delta t_{decrease}$, δ_1, δ_2, $\Delta t_{increase}$. Initial parameter values were estimated based on visual inspection of torque data. Through multiple iterations of the tuning set, optimal values for parameters were identified, enabling accurate detection of breaches at the most opportune moment. Below is the proposed pseudo-algorithm for preventing potential breaches during pedicle drilling (Algo. 1).

Algorithm 1 Bone breach detection.

Input: τ, raw cutting torque in Newton meters
Input: t, time in seconds
Input: z, depth insertion in the bone in millimeters
Output: $Alert$, breach detected

$c_t = Chebyshev(\tau, (n = 4, r_p = 0.5, w = 0.03))$
$c'(t) = \frac{dc(t)}{dt}$
if
$$\forall t_n \in [t - \Delta t_{decrease}, t] : c'(t_n) < 0$$
then
  t_x is the time t when the derivative $c' = 0$
  $t_i = t_x - \Delta t_{increase}$
  $d = c_{tx} - c_{t_i}$
  if $(c'(t) < \delta_1$ & $d > \delta_2)$ **then**
    $Alert \leftarrow \mathbf{True}$
  end if
end if

V. VALIDATION AND ANALYSIS

The methods and materials proposed have been evaluated on 80 fresh pig vertebrae collected from the butcher. For each vertebra, we performed an intentional spinal canal perforation using our robotic setup equipped with the driller. Then, we emulated real-time vertebra drilling by replaying the signals, performing online data filtering and detecting breaches.

A. Parameters Optimization and Validation

Part of the recorded data (i.e., 30%) was used as tunning data to estimate off-line the parameters of our algorithm. After 16,800 iterations, the optimization process yields the parameters shown in Table I. These parameters assume an error stop of +2 mm after the very beginning of the breach (i.e., deformation of periosteal tissue, as can be seen in Fig. 5(b)) and 5 mm before the breach.

TABLE I
PARAMETERS USED TO TRIGGER BREACH DETECTION CONDITIONS

Definition	Parameter	Parameter value
Downward Slope Interval	$\Delta t_{decrease}$	$0.4s$
The minimum value of slope after downward slope interval	δ_1	$-0.3N \cdot m/s$
Interval during which the signal increases progressively	$\Delta t_{increase}$	$10s$
Increase in torque during $\Delta t_{increase}$	δ_2	$80N \cdot m$

The proposed algorithm (Algo. 1) was first evaluated in the set of data used to tune the algorithm's parameters given in Table I to ensure that our method works on this data before evaluating it on the rest of data (i.e., 70%) that has not been processed. It has been demonstrated that the breach detection algorithm provides an average detection error of $\overline{e}_{\text{tuning}}$ = -0.05 mm $\pm$ 1.32 mm. The maximum and minimum error were $\min(e_{tuning})$ = -1.42 mm and $\max(e_{tuning})$ = 3.47 mm, respectively. Figure 7 depicts the breach detection errors on the part of the data used to estimate the algorithm's parameters. As expected, the algorithm detects the breach in 100% of cases (i.e., 24/24 vertebrae).

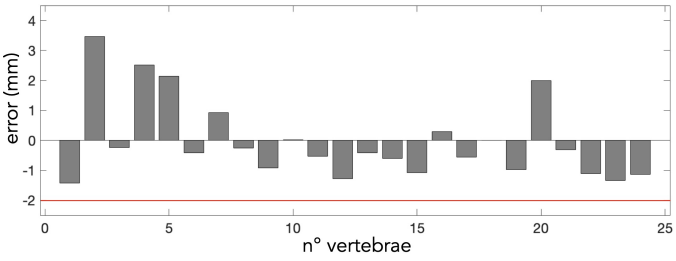

Fig. 7. Barplot illustrating the algorithm's results on the tuning set. The shaded area represents the accepted limits, with errors less than -2 mm considered breaches and errors greater than 5mm considered premature detections.

Afterwards, the method was applied to the validation set with the same parameters as the tuning set. The algorithm achieved breach detection with a mean error $\overline{e}_{\text{validation}}$ = 0.26 $\pm$ 2.36 mm. The minimum and maximum error were $\min(e_{validation})$ = -1.96 mm and $\max(e_{validation})$ = 11.28 mm, respectively. Figure 8 depicts the breach detection errors on the validation set (i.e., the remaining 70%) for each drilled vertebra. There were only two cases with error $e > 5$ mm. The first case was the pedicle with the error of 11.28 mm (vertebra n°21). After investigation using a post-drilling CT scan, it was found that this vertebra exhibits a breach outside the canal on the lamina because the surgeon had not defined the drilling trajectory with sufficient precision, as shown in Fig. 9. The second case corresponds to the vertebrae n°7 where the detection error is slightly superior to 5 mm. Due to the pronounced medial trajectory, the drill encountered the cortical bone of the lamina, precipitating an early detection akin to breaching the cortical bone of the spinal canal. Figure 10 illustrates the premature breach detection (from top to bottom: post-drilling CT scan, torque signal and drill bit depth measurement).

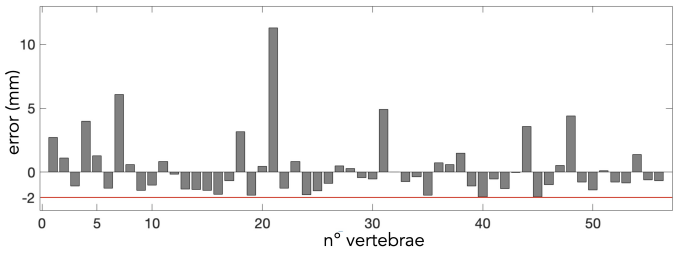

Fig. 8. Barplot illustrating the breach detection error for each drilled pedicle for the validation data set.

As a result, the average breach detection error throughout the validation set is estimated to be $\overline{e}_{\text{validation}}$ = -0.06 mm $\pm$ 1.84 mm, with a minimum and a maximum error of $\min(e_{validation})$ = -1.96 mm and $\max(e_{validation})$ = 11.28 mm (corresponding to the breach detection on the cortical (Fig. 9)), respectively. These results show that using torque as a signal to prevent a potential breach in the spinal canal is efficient (96.42% of success), with the capacity to identify the breach relatively far upstream.

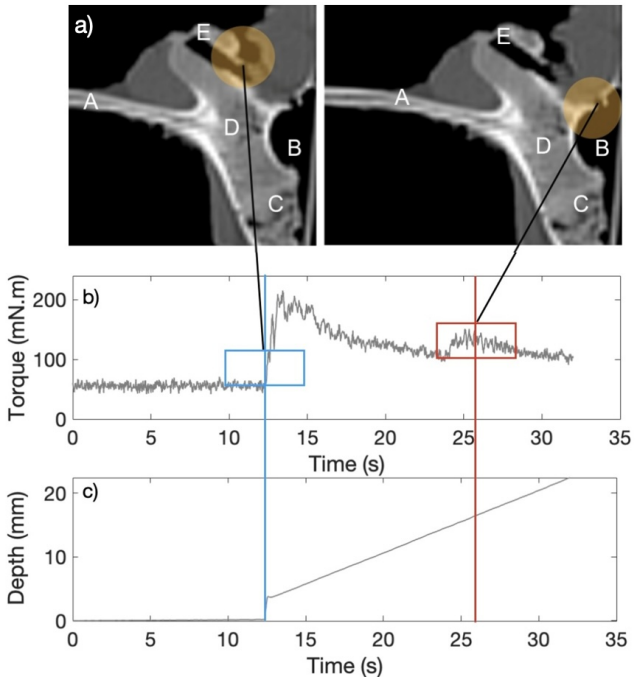

Fig. 9. Illustration of the case of vertebra n°21, where the trajectory defined by the surgeon allowed for a breach not in the spinal canal but outside the pedicle. Our algorithm was still able to detect the involved breach out of the cortex. The blue line indicates the breach detected by the algorithm outside the vertebra body, and the red one depicts the breach in the spinal canal. **A**: transverse process, **B**: spinal canal, **C**: vertebral body, **D**: pedicle, and **E**: drilling trajectory.

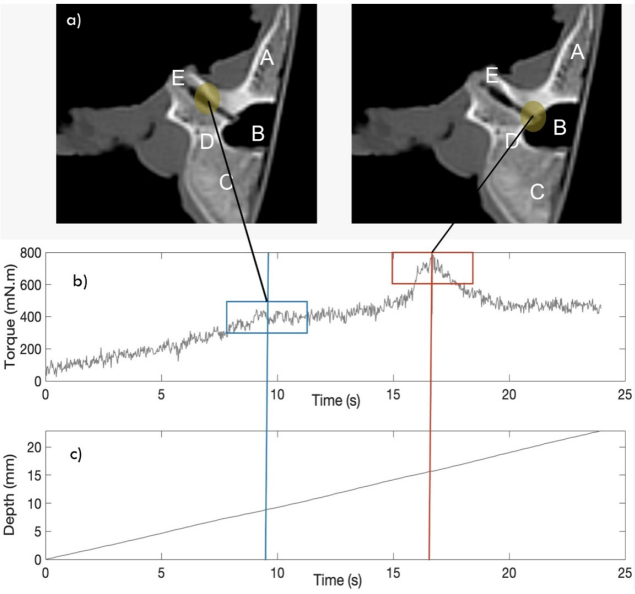

Fig. 10. Example of a vertebra (n° 6) exhibiting premature detection due to the presence of cortical bone within the pedicle, coupled with an excessively medial trajectory. **A**: transverse process, **B**: spinal canal, **C**: vertebral body, **D**: pedicle, and **E**: drilling trajectory. The blue line represents the first torque peak indicating engagement with cortical bone, which occurs at ≈7 mm from the entry point. The red line depicts the second torque peak, signifying engagement with cortical bone in the spinal canal, which occurs at ≈14 mm from the entry point.

B. Angle Correlation

Historically, the influence of drilling angle on torque-based methods for detecting cortical bone perforation remained elu-

sive. This ambiguity stemmed from the theoretical dependence of torque on the extent of drill thread engagement with the bone. Given that this engagement is directly impacted by the angle between the drill axis and the cortical bone surface, a clear understanding of this relationship was crucial. To quantify the impact of drilling angle on torque-based detection, we employed a robust correlation analysis, specifically examining the relationship between drill-cortical bone angle and the accuracy of cortical bone breach identification. To do this, a millimetre-scale CT scan conducted after the experiment detailed the desired orientation relative to surrounding structures. The penetration angle is between the desired trajectory and the spinal canal. It is defined by the angle between the desired trajectory and the tangent to the spinal canal at the penetration point (Fig. 11).

This study pointed out the mean of the drilling angle $\overline{a} = 66.24° \pm 18.26°$. The drilling angle and detection correlation are weak, with a Pearson correlation coefficient r = 0.16 and p-value = 0.15.

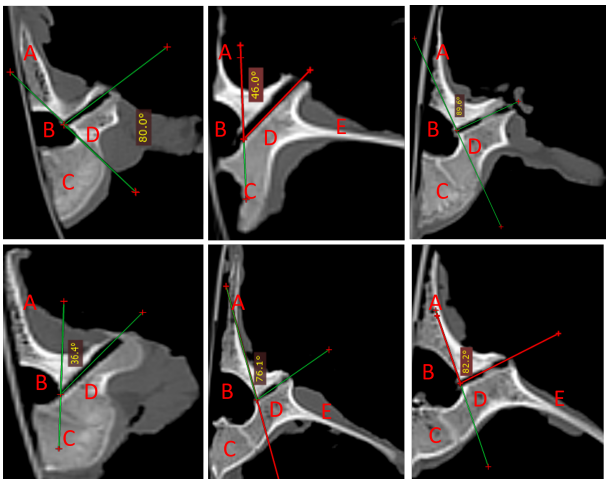

Fig. 11. Examples of the measurement of the angle between the aimed trajectory and the spinal canal. **A**: spinous process, **B**: medullary canal, **C**: vertebral body, **D**: pedicle, and **E**: transverse process.

C. Limitations and beyond Pedicle Screws Placement

First, our breach detection algorithm was evaluated in data recorded during the drilling of 80 fresh pig vertebrae collected from the butcher. The transposability of this method to a living subject requires several parameters to be taken into account. The bone density of vertebrae can vary from one group of subjects to another, for example, from the elderly to younger patients. It is widely acknowledged that the dimensions and bone density of porcine pedicles differ from those of humans. Furthermore, bone size and density variations are observed among individuals of different ages and statures within the human population. Additionally, there can be variability between lumbar and thoracic vertebrae even within the same individual. However, a consistent feature is the transition from less dense cancellous bone to cortical bone. As a result, some of the method parameters can vary, although the pattern of the drilling torque signal remains similar. To remedy this, certain parameters can be redefined according to age groups, a calibration-like procedure. Another phenomenon that can affect the correct functioning of the breach detection algorithm is the movement of the spine (i.e., due to breathing) and, therefore, of the vertebrae during the drilling procedure. However, the force control law proposed in Section III-B, thanks to its good dynamics, keeps the drill head and pedicle in constant contact, which means intuitively compensating for breathing-induced movements. In scoliotic surgery, pedicle sclerosis in the concavity may affect the detection ability. In such cases, a multi-sensor approach may be required. These findings warrant further evaluation and validation in patient populations.

The proposed robotic platform and breach detection algorithm can have other applications beyond pedicle screw placement. In neurology and otology surgeries, drilling near critical structures like nerves and blood vessels requires a breach detection method to stop the drilling procedure automatically in the early stages of bone inner wall fracture. Traumatology often requires the placement of screws to manage complex fractures or reconstruction of shattered bones. A real-time breach detection algorithm can help the surgeon to safely secure bone fragments with screws and plates, avoiding additional damage to the bone or surrounding tissues.

VI. DISCUSSION AND CONCLUSION

Real-time breach detection is a challenging procedure. In spine surgery, breaches will lead to tissue damage. Breaches measuring less than 2 mm (i.e., grades "*A*" to "*B*") pose a low risk to the patient [2]. This work aims to mitigate breaches beyond grade "*B*". The torque is an accurate signal that can be used to establish an algorithm for breach detection. Given the inherent noise in the cutting torque signal, it is essential to utilize a filter such as *Chebyshev* filters to reduce the noise and extract only meaningful trends from the signal.

This study set the acceptable error range with a lower limit of -2 mm to prevent breaches exceeding grade "B". The upper limit was set at 5 mm to enable early detection and timely adjustment of the target direction. Breaches detected before reaching 5 mm were classified as premature or false positives. It can be asserted that the detection capability remains unaffected by the drilling angle. Therefore, our detection ability remained effective even with more tangential approaches. This is significant, as the aim is typically not perpendicular to the canal in actual surgical scenarios.

This work is the first to demonstrate real-time breach detection using torque with ground truth data made by a surgeon. While previous research has illustrated the feasibility of this task in offline settings [45], our study showcased its successful implementation in real-time scenarios. Nevertheless, validation on deformed human vertebrae, such as those from patients with scoliosis, is still needed, as their anatomical models can differ significantly from those of animals.

In conclusion, the implementation of a comprehensive sensor integration emerges as an optimal solution to enhance safety in spinal surgery. By combining various sensors, we can create a multifaceted safety system that addresses diverse

aspects of the surgical environment. This approach ensured a more robust and reliable detection mechanism and provided a broader spectrum of information, improving surgical safety measures overall.

Future work will involve transposing the breach detection algorithm in experimental conditions close to those of an operating room, e.g., on an animal model (pig) subject to breathing motions.

REFERENCES

[1] W. Skalli et al., "Quantification of three-dimensional vertebral rotations in scoliosis: what are the true values?" Spine, vol. 20, no. 5, pp. 546–553, 1995.

[2] S. D. Gertzbein and S. E. Robbins, "Accuracy of pedicular screw placement in vivo." Spine, vol. 15, no. 1, pp. 11–14, 1990.

[3] J.-M. Mac-Thiong, S. Parent, et al., "Neurological outcome and management of pedicle screws misplaced totally within the spinal canal," Spine, vol. 38, no. 3, pp. 229–237, 2013.

[4] Y. Ogura, K. Watanabe, N. Hosogane, et al., "Acute respiratory failure due to hemothorax after posterior correction surgery for adolescent idiopathic scoliosis: a case report," BMC Musculoskeletal Disorders, vol. 14, no. 1, pp. 1–4, 2013.

[5] J. B. Choi, J. O. Han, et al., "False aneurysm of the thoracic aorta associated with an aorto-chest wall fistula after spinal instrumentation," J. of Trauma and Acute Care Surg., vol. 50, no. 1, pp. 140–143, 2001.

[6] M. E. Minor, N. J. Morrissey, R. Peress, A. Carroccio, S. Ellozy, G. Agarwal, V. Teodorescu, L. H. Hollier, and M. L. Marin, "Endovascular treatment of an iatrogenic thoracic aortic injury after spinal instrumentation: case report," J. of vascular Surg., vol. 39, no. 4, pp. 89x3–896, 2004.

[7] B. Wegener, C. Birkenmaier, A. Fottner, V. Jansson, and H. R. Dürr, "Delayed perforation of the aorta by a thoracic pedicle screw," Eu. Spine J., vol. 17, pp. 351–354, 2008.

[8] M. K. Kwan, C. K. Chiu, S. M. Abd Gani, and C. C. Y. Wei, "Accuracy and safety of pedicle screw placement in adolescent idiopathic scoliosis patients: a review of 2020 screws using computed tomography assessment," Spine, vol. 42, no. 5, pp. 326–335, 2017.

[9] M. Di Silvestre, P. Parisini, F. Lolli, and G. Bakaloudis, "Complications of thoracic pedicle screws in scoliosis treatment," Spine, vol. 32, no. 15, pp. 1655–1661, 2007.

[10] A. Y. Şarlak, B. Tosun, H. Atmaca, H. T. Sarisoy, and L. Buluç, "Evaluation of thoracic pedicle screw placement in adolescent idiopathic scoliosis," Eu. Spine J., vol. 18, pp. 1892–1897, 2009.

[11] G. Rao, D. S. Brodke, M. Rondina, and A. T. Dailey, "Comparison of computerized tomography and direct visualization in thoracic pedicle screw placement," J. of Neurosurg.: Spine, vol. 97, pp. 223–226, 2002.

[12] E. D. Sheha, S. D. Gandhi, and M. W. Colman, "3d printing in spine surgery," Ann. of translational medicine, vol. 7, no. Suppl 5, 2019.

[13] A. Senkoylu, I. Daldal, and M. Cetinkaya, "3d printing and spine surgery," J. of Orthop. Surg., vol. 28, no. 2, p. 2309499020927081, 2020.

[14] E. Saghbiny, J. Da Silva, C. Chaimi, et al., "Protocol for electrical conductivity signal collection and processing in scoliosis surgery," Adv. in Orthop., vol. 2023, 2023.

[15] L. Leblanc, E. Saghbini, etãl, "Automatic spinal canal breach detection during pedicle screw placement," IEEE Robotics and Automation Letters, vol. 9, pp. 1915–1922, 2024.

[16] B. De Vega, A. R. Navarro, A. Gibson, and D. M. Kalaskar, "Accuracy of pedicle screw placement methods in pediatrics and adolescents spinal surgery: a systematic review and meta-analysis," Global Spine J., vol. 12, no. 4, pp. 677–688, 2022.

[17] Z.-X. Wu, L.-y. Huang, et al., "Accuracy and safety assessment of pedicle screw placement using the rapid prototyping technique in severe congenital scoliosis," Clin. Spine Surg., vol. 24, pp. 444–450, 2011.

[18] Y.-S. Bai, Y.-F. Niu, Z.-Q. Chen,et al., "Comparison of the pedicle screws placement between electronic conductivity device and normal pedicle finder in posterior surgery of scoliosis," Clin. Spine Surg., vol. 26, pp. 316–320, 2013.

[19] L. A. Tan, K. Yerneni, A. Tuchman, et al., "Utilization of the 3d-printed spine model for freehand pedicle screw placement in complex spinal deformity correction," J. of Spine Surg., vol. 4, no. 2, p. 319, 2018.

[20] P. Su, W. Zhang, Y. Peng, et al., "Use of computed tomographic reconstruction to establish the ideal entry point for pedicle screws in idiopathic scoliosis," Eu. Spine J., vol. 21, pp. 23–30, 2012.

[21] A. Perdomo-Pantoja, W. Ishida, C. Zygourakis, et al., "Accuracy of current techniques for placement of pedicle screws in the spine: a comprehensive systematic review and meta-analysis of 51,161 screws," World neurosurgery, vol. 126, pp. 664–678, 2019.

[22] N. Rawicki, J. E. Dowdell, and H. S. Sandhu, "Current state of navigation in spine surgery," Ann. of Transl. Med., vol. 9, 2021.

[23] P. Merloz, J. Troccaz, H. Vouaillat, et al. "Fluoroscopy-based navigation system in spine surgery," J. of Eng. in Med., vol. 221, no. 7, pp. 813–820, 2007.

[24] J. D. Mathews, A. V. Forsythe, et al., "Cancer risk in 680 000 people exposed to computed tomography scans in childhood or adolescence: data linkage study of 11 million australians," Bmj, vol. 346, 2013.

[25] H. Yan, D. Jiang, L. Xu, et al., "Does the full power-assisted technique used in pedical screw placement affect the safety and efficacy of adolescent idiopathic scoliosis surgery?" World Neurosurgery, vol. 116, pp. e79–e85, 2018.

[26] D. A. Seehausen, D. L. Skaggs, L. M. Andras, and Y. Javidan, "Safety and efficacy of power-assisted pedicle tract preparation and screw placement," Spine Deformity, vol. 3, pp. 159–165, 2015.

[27] H. Clement, N. Heidari, W. Grechenig, et al., "Drilling, not a benign procedure: laboratory simulation of true drilling depth," Injury, vol. 43, no. 6, pp. 950–952, 2012.

[28] M. H. Aziz, M. A. Ayub, and R. Jaafar, "Real-time algorithm for detection of breakthrough bone drilling," Procedia Eng., vol. 41, pp. 352–359, 2012.

[29] W.-Y. Lee and C.-L. Shih, "Control and breakthrough detection of a three-axis robotic bone drilling system," Mechatronics, vol. 16, no. 2, pp. 73–84, 2006.

[30] P. Brett, D. Baker, L. Reyes, and J. Blanshard, "An automatic technique for micro-drilling a stapedotomy in the flexible stapes footplate", J. of Eng. in Med., vol. 209, no. 4, pp. 255–262, 1995.

[31] Y. Torun and A. Öztürk, "A new breakthrough detection method for bone drilling in robotic orthopedic surgery with closed-loop control approach," Ann. of Biomed. Eng., vol. 48, no. 4, pp. 1218–1229, 2020.

[32] W. Wang, Y. Shi, N. Yang, and X. Yuan, "Experimental analysis of drilling process in cortical bone," Medical Eng. & Phys., vol. 36, pp. 261–266, 2014.

[33] V. Zakeri and A. J. Hodgson, "Classifying hard and soft bone tissues using drilling sounds," in IEE Int. Conf. Eng. in Med. and Bio. Soc., 2017, pp. 855–858.

[34] V. Zakeri and A. J. Hodgson, "Automatic identification of hard and soft bone tissues by analyzing drilling sounds," IEEE/ACM Trans. on Audio, Spee., and Lang. Proc., vol. 27, no. 2, pp. 404–414, 2018.

[35] D. Yu, X. Yuan, and Z. Jianxun, "State identification based on sound analysis during surgical milling process," in IEEE Int. Conf. on Rob. and Biomem., 2015, pp. 1666–1669.

[36] Y. Sun, H. Jin, Y. Hu, et al., "State recognition of bone drilling with audio signal in robotic orthopedics surgery system," in IEEE/RSJ Int. Conf. on Intel. Rob. and Syst., 2014, pp. 3503–3508.

[37] F. Guan, Y. Sun, X. Qi, et al., "State recognition of bone drilling based on acoustic emission in pedicle screw operation," Sensors, vol. 18, no. 5, p. 1484, 2018.

[38] M. Seibold et al., "Real-time acoustic sensing and artificial intelligence for error prevention in orthopedic surgery", Sci Rep, vol. 11, no. 1, p. 9638, 2021

[39] A. Massalimova, M. Timmermans, N. Cavalcanti, et al., "Automatic breach detection during spine pedicle drilling based on vibroacoustic sensing," arXiv preprint arXiv:2303.15114, 2023.

[40] M. Timmermans, A. Massalimova, R. Li, et al., "State-of-the-art of non-radiative, non-visual spine sensing with a focus on sensing forces, vibrations and bioelectrical properties: A systematic review," Sensors, vol. 23, no. 19, p. 8094, 2023.

[41] N. Hogan, "On the stability of manipulators performing contact tasks," IEEE J. on Rob. and Auto., 1988.

[42] T. Lasky and T. Hsia, "On force-tracking impedance control of robot manipulators" in Int. Conf. on Rob. and Auto., 1991, pp. 274–280.

[43] J. D. Silva, S. Vafadar, T. Chandanson, et al., "Force control of the KUKA LBR Med without external force sensor," 11 ed. of CRAS, 2022.

[44] L. Weinberg and P. Slepian, "Takahasi's results on tchebycheff and butterworth ladder networks," IRE Trans. on Circuit Theory, vol. 7, no. 2, pp. 88–101, 1960.

[45] E. Saghbiny, J. Da Silva, L. Leblanc, et al., "Breach detection in spine surgery based on cutting torque with ex-vivo experimental validation," in 12 ed. of CRAS, 2023.